Heuristic Variable Switching Point Predictive Current Control for the Three-Level Neutral Point Clamped Inverter

Peter Stolze*, Petros Karamanakos†, Males Tomlinson‡, Ralph Kennel*, Toit Mouton‡ and Stefanos Manias†

*Institute for Electrical Drive Systems and Power Electronics, Technische Universität München, Munich, Germany
Email: *peter.stolze@tum.de, ralph.kennel@tum.de
†Department of Electrical and Computer Engineering, National Technical University of Athens, Athens, Greece
Email: †petkar@central.ntua.gr, manias@central.ntua.gr
‡Department of Electrical and Electronic Engineering, University of Stellenbosch, Stellenbosch, South Africa
Email: ‡tomlindm@eskom.co.za, dtmouton@sun.ac.za

***Abstract*—This paper presents a variable switching point predictive current control (VSP^{2}CC) method for induction machines (IMs) driven by a three-level neutral point clamped (NPC) inverter with a heuristic preselection of the optimal voltage vector. Enumeration-based model predictive control (MPC) methods are very simple, easy to understand and, in general, offer the possibility to control any nonlinear system with arbitrary user-defined terms in the cost function. However, the two most important drawbacks are the increased computational effort which is required and the high ripples on the controlled variables which limit the applicability of these methods. These high ripples result from the fact that in enumeration-based MPC algorithms the actuating variable can only be changed at the *beginning* of a sampling interval. However, by changing the applied voltage vector *within* the sampling interval, a voltage vector can be applied for a shorter time than one sample, which results in a reduced ripple. Since this strategy leads to an additional overhead which is crucial especially for multilevel inverters, it is combined with a heuristic preselection of the optimal voltage vector to reduce the calculation effort. Experimental results are provided to verify the proposed strategy. Furthermore, it will be shown experimentally that a conventional enumeration-based MPC method will lead to very low switching frequencies and high current ripples at low machine speeds; this significant drawback can be overcome with the proposed VSP^{2}CC strategy.**

I. Introduction

Today, field oriented control (FOC) [1] and direct torque control (DTC) [2], [3] are mostly used for controlling three-phase electrical machines. FOC makes use of modulators, whereas DTC utilizes hysteresis controllers for both flux and torque, and outputs a switching state which is directly commanded to the inverter. Because of the absence of a modulator, DTC is known to show a faster transient response than FOC, whereas it normally produces higher current, flux and torque ripples.

Although model predictive control (MPC) [4], [5] methods have been widely used for more than 40 years in process and chemical engineering, the application of such strategies to electrical drive systems and power electronics has just recently been gaining more popularity [6]–[13]. MPC-based algorithms can be divided into modulation-based and enumeration-based MPC strategies [14]–[17]. The two main drawbacks of enumeration-based MPC methods are the high computational complexity due to the complete enumeration of all control inputs, i.e. the switching states, and the high ripples on the controlled variables compared to modulation-based approaches.

With regards to the first problem, in [18] a heuristic voltage vector preselection has been proposed that can be effectively applied to MPC schemes where a longer prediction horizon is required, since it can significantly reduce the necessary computations. Furthermore, as shown in [19], this strategy can be successfully applied to the current control loop of induction machines (IMs).

The second problem of enumeration-based strategies comes from the fact that a switching state is applied for *at least* one whole sampling interval, resulting in high ripples. If a modulator is used, active voltage vectors which in general lead to higher ripples than the zero ones can be applied for a much shorter time. Hence, in order to reduce ripples on the controlled variables, in [20]–[22] an MPC strategy, called variable switching point predictive torque control (VSP^{2}TC), was introduced showing promising results. According to this algorithm, a variable switching point (VSP) in time t_{sw}, with

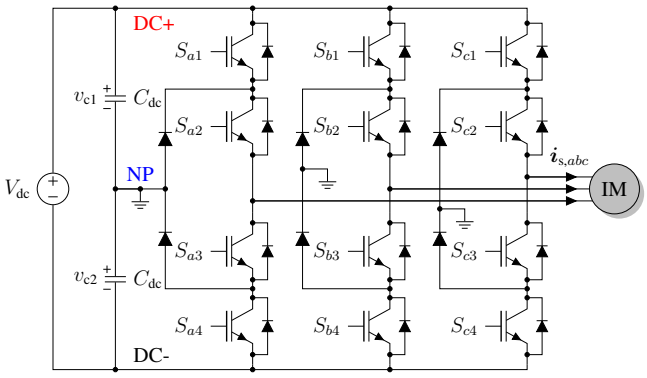

Fig. 1. Three-level neutral point clamped (NPC) voltage source inverter driving an induction machine (IM).

$0 \leq t_{\mathrm{sw}} \leq T_{\mathrm{s}}$, where T_{s} is the sampling interval, is calculated in order to minimize the torque ripple. However, it should be mentioned that calculating a VSP further increases the computational burden, resulting in a limited applicability of such methods, especially for multilevel inverters.

To overcome the previously mentioned drawbacks of enumeration-based methods, in this paper the basic principle that was used for the torque ripple minimization in VSP^{2}TC is applied to the current control loop of an IM. Furthermore, the proposed VSP strategy is combined with a heuristic preselection of the optimal voltage vector so as to reduce the required computations. In a first step the continuous-valued solution of the optimization problem (assuming that the continuous-valued voltage vector is applied for a *whole* sampling interval) is determined. Then, the three discrete-valued voltage vectors that can be produced by the inverter and which are closest to this continuous-valued optimum are considered for the MPC algorithm. Subsequently, an optimization problem is formulated according to which a VSP is calculated such that the squared rms current error for both α and β components of the stator current $\boldsymbol{i}_{\mathrm{s}}$ is minimized. In this way, current ripples can be effectively reduced and the necessary calculation effort is even less compared to a complete enumeration of all possible voltage vectors.

Moreover, the presented control scheme comes with an additional advantage. In general, for enumeration-based methods the real switching frequency per device is much lower than half the sampling frequency, while it also highly depends on the operating point. Especially at low machine speeds the switching frequency per IGBT can reach values around 100 Hz whereas it can be several kHz at higher speeds. The proposed method increases the switching frequency, especially at these operating points, and delivers significantly improved currents while not affecting the dynamic response of the system.

The introduced algorithm is applied to an IM fed by a three-level neutral point clamped (NPC) inverter. In addition, the necessary dc-link voltage balancing algorithm can be easily included into the cost function. It should be pointed out that the proposed strategy is very promising for low-voltage (LV) drives where, in contrast to medium- (MV) and high-voltage (HV) drives, a good quality of the controlled variables is much more important than low switching frequencies.

The paper is organized as follows: Section II gives an overview of the physical system; in Section III the control algorithm with heuristic preselection and the VSP calculation is described. Section IV contains experimental results to verify the proposed method and in Section V the conclusion and an outlook to further work is given.

II. Physical System

A. Three-Level NPC Inverter

Fig. 1 shows the three-level NPC inverter connected to an IM. DC+ and DC- are the positive and negative dc-link rails, respectively. NP is the neutral (zero) point. Ideally, the two dc-link capacitor voltages v_{c1} and v_{c2} are equal to $0.5V_{\mathrm{dc}}$, where V_{dc} is the dc-link voltage. Every phase has two complementary pairs of switches (S_{j1}/S_{j3} and S_{j2}/S_{j4}, $j = \{a, b, c\}$), i.e. if

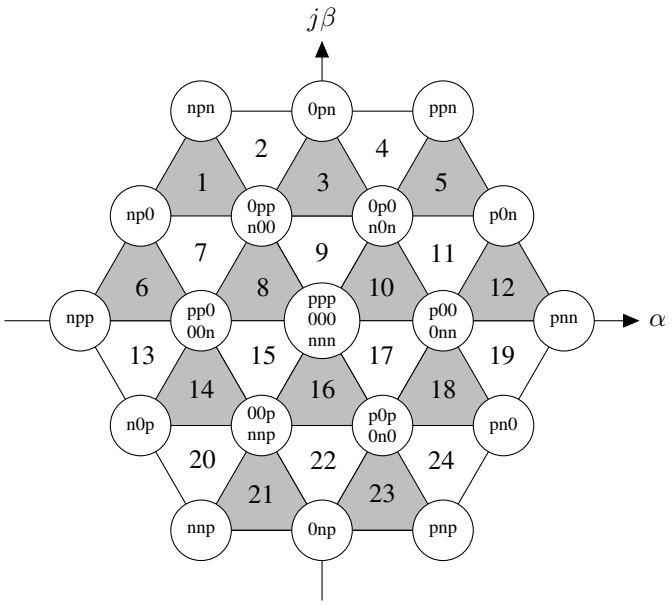

Fig. 2. Voltage vectors of a three-level NPC inverter and the corresponding switching states

one of the two complementary switches is *on*, the other one has to be *off* and vice versa. The inverter can produce the voltages $-0.5V_{\mathrm{dc}}$, 0 V and $0.5V_{\mathrm{dc}}$ in every phase. This leads to $3^3 = 27$ switching possibilities which are modeled with $-1, 0, 1$ corresponding to the phase voltages $-0.5V_{\mathrm{dc}}$, 0 V and $0.5V_{\mathrm{dc}}$, respectively.

By using the Clarke transformation, a variable in the three-phase abc system ($\boldsymbol{\xi}_{abc} = [\xi_a\ \xi_b\ \xi_c]^T$) can be transformed to $\boldsymbol{\xi}_{\alpha\beta} = [\xi_\alpha\ \xi_\beta]^T$ in an equivalent but linearly independent $\alpha\beta$ coordinate system, resulting in 19 unique voltage vectors (see Fig. 2—positive switching states are denoted with p, negative ones with n), through $\boldsymbol{\xi}_{\alpha\beta} = \boldsymbol{K}\boldsymbol{\xi}_{abc}$, with

$$\boldsymbol{K} = \frac{2}{3}\begin{bmatrix} 1 & -\frac{1}{2} & -\frac{1}{2} \\ 0 & \frac{\sqrt{3}}{2} & -\frac{\sqrt{3}}{2} \end{bmatrix}. \tag{1}$$

As already mentioned, the two dc-link capacitor voltages shown in Fig. 1 have to be close to their reference values of $0.5V_{\mathrm{dc}}$. However, if a current is drawn from the neutral point, these voltages will change. Thus, a voltage balancing algorithm has to be implemented in order to keep these voltages balanced. In other words, the voltage difference should be

$$\Delta v_{\mathrm{c}} = v_{\mathrm{c1}} - v_{\mathrm{c2}} = 0\,. \tag{2}$$

Note that positive or negative switching states do not affect the voltage balance. By applying Kirchhoff's current law and utilizing the differential equation of a capacitor, the neutral point voltage balancing mechanism can be described by

$$\frac{\mathrm{d}\Delta v_c}{\mathrm{d}t} = \frac{1}{C_{\mathrm{dc}}} \sum_{j=a,b,c} i_{\mathrm{n}j}\,, \tag{3}$$

where $i_{\mathrm{n}j}$ is the neutral point current in phase j. This current is equal to the phase current if a zero switching state is applied in this phase, otherwise it is zero.

B. Induction Machine

According to [23] the basic equations of an IM can be written in a coordinate system which rotates with an arbitrary angular velocity ω_k as

$$\boldsymbol{\psi}_\mathrm{s} = l_\mathrm{s}\boldsymbol{i}_\mathrm{s} + l_\mathrm{m}\boldsymbol{i}_\mathrm{r}\,, \tag{4a}$$

$$\boldsymbol{\psi}_\mathrm{r} = l_\mathrm{m}\boldsymbol{i}_\mathrm{s} + l_\mathrm{r}\boldsymbol{i}_\mathrm{r}\,, \tag{4b}$$

$$\boldsymbol{v}_\mathrm{s} = r_\mathrm{s}\boldsymbol{i}_\mathrm{s} + \frac{\mathrm{d}\boldsymbol{\psi}_\mathrm{s}}{\mathrm{d}t} + j\omega_\mathrm{k}\boldsymbol{\psi}_\mathrm{s}\,, \tag{4c}$$

$$\boldsymbol{v}_\mathrm{r} = r_\mathrm{r}\boldsymbol{i}_\mathrm{r} + \frac{\mathrm{d}\boldsymbol{\psi}_\mathrm{r}}{\mathrm{d}t} + j(\omega_\mathrm{k} - \omega_\mathrm{r})\boldsymbol{\psi}_\mathrm{s}\,. \tag{4d}$$

Stator variables are marked in the form $(*)_\mathrm{s}$ while rotor variables are denoted in the way $(*)_\mathrm{r}$. $\boldsymbol{\psi}_\mathrm{s}$ and $\boldsymbol{\psi}_\mathrm{r}$ are the fluxes, $\boldsymbol{i}_\mathrm{s}$ and $\boldsymbol{i}_\mathrm{r}$ the currents, r_s and r_r the resistances, l_s and l_r the inductances and l_m is the mutual inductance between stator and rotor. $\boldsymbol{v}_\mathrm{s}$ is the applied stator voltage and $\boldsymbol{v}_\mathrm{r}$ the rotor voltage ($\boldsymbol{v}_\mathrm{r} = 0$ for a squirrel-cage IM). j is defined as $j = \sqrt{-1}$. ω_r is the rotor rotational speed

$$\omega_\mathrm{r} = p\omega_\mathrm{m}\,, \tag{5}$$

where p is the number of pole pairs and ω_m is the mechanical machine speed.

For $\omega_\mathrm{k} = 0$ the coordinate system is stator-fixed, i.e. the coordinates are given in the $\alpha\beta$ system. In order to obtain a more compact system representation, it is quite common to describe the $\alpha\beta$ system with complex numbers where the real part corresponds to the α axis and the imaginary part to the β axis.

According to [24], (4) can be rewritten in the form

$$\tau_\sigma\frac{\mathrm{d}\boldsymbol{i}_\mathrm{s}}{\mathrm{d}t} + \boldsymbol{i}_\mathrm{s} = -j\omega_\mathrm{k}\tau_\sigma\boldsymbol{i}_\mathrm{s} + \frac{k_\mathrm{r}}{r_\sigma}\Big(\frac{1}{\tau_\mathrm{r}} - j\omega_\mathrm{r}\Big)\boldsymbol{\psi}_\mathrm{r} + \frac{1}{r_\sigma}\boldsymbol{v}_\mathrm{s}\,, \tag{6a}$$

$$\tau_\mathrm{r}\frac{\mathrm{d}\boldsymbol{\psi}_\mathrm{r}}{\mathrm{d}t} + \boldsymbol{\psi}_\mathrm{r} = -j(\omega_\mathrm{k} - \omega_\mathrm{r})\tau_\mathrm{r}\boldsymbol{\psi}_\mathrm{r} + l_\mathrm{m}\boldsymbol{i}_\mathrm{s}\,, \tag{6b}$$

where the coefficients are given by $\tau_\sigma = \frac{\sigma l_\mathrm{s}}{r_\sigma}$ and $r_\sigma = r_\mathrm{s} + k_\mathrm{r}^2 r_\mathrm{r}$ with $k_\mathrm{r} = \frac{l_\mathrm{m}}{l_\mathrm{r}}$, $\tau_\mathrm{r} = \frac{l_\mathrm{r}}{r_\mathrm{r}}$ and $\sigma = 1 - \frac{l_\mathrm{m}^2}{l_\mathrm{s} l_\mathrm{r}}$.

The mechanical machine torque is given by

$$T_\mathrm{m} = \frac{3}{2}p(\boldsymbol{\psi}_\mathrm{s} \times \boldsymbol{i}_\mathrm{s}) = \frac{3}{2}p(\boldsymbol{\psi}_\mathrm{r} \times \boldsymbol{i}_\mathrm{r}). \tag{7}$$

Finally, the mechanical differential equation can be stated as

$$\frac{\mathrm{d}\omega_\mathrm{m}}{\mathrm{d}t} = \frac{1}{J}(T_\mathrm{m} - T_\ell) \tag{8}$$

where T_ℓ is the mechanical load torque and J the inertia.

III. Heuristic Variable Switching Point Predictive Current Control (VSP^{2}CC)

A. Stator Current Equations

First, the continuous-time equations for the stator current have to be developed. (6a) can be rewritten as

$$\frac{\mathrm{d}\boldsymbol{i}_\mathrm{s}}{\mathrm{d}t} = -\frac{1}{\tau_\sigma}\boldsymbol{i}_\mathrm{s} + \frac{1}{r_\sigma\tau_\sigma}(\boldsymbol{v}_\mathrm{s} - \boldsymbol{v}_\mathrm{emf})\,, \tag{9}$$

with the back-EMF voltage

$$\boldsymbol{v}_\mathrm{emf} = -k_\mathrm{r}(\frac{1}{\tau_\mathrm{r}} - j\omega_\mathrm{r})\boldsymbol{\psi}_\mathrm{r}\,. \tag{10}$$

For the rotor flux estimation (6b) is used ($\omega_\mathrm{k} = 0$):

$$\tau_\mathrm{r}\frac{\mathrm{d}\boldsymbol{\psi}_\mathrm{r}}{\mathrm{d}t} + \boldsymbol{\psi}_\mathrm{r} = j\omega_\mathrm{r}\tau_\mathrm{r}\boldsymbol{\psi}_\mathrm{r} + l_\mathrm{m}\boldsymbol{i}_\mathrm{s}\,. \tag{11}$$

As it can be seen from (9), the current control loop is a linear first-order system with an external disturbance. The back-EMF voltage $\boldsymbol{v}_\mathrm{emf}$ is changing slowly over the sampling interval and hence, it can be assumed as constant for the whole prediction horizon.

By using the forward Euler approximation, the equations for current prediction, back-EMF and rotor flux estimation, as given by (9), (10), and (11), respectively, can be discretized with the sampling interval T_s.

B. Block Diagram of the Control Algorithm

Fig. 3 shows the block diagram of the proposed variable switching point predictive current control (VSP^{2}CC) algorithm with heuristic voltage vector preselection. As the three phase currents in the machine are balanced, only two of them have to be measured. Furthermore, it is necessary to measure the machine speed. The torque reference is generated by a conventional speed proportional-integral (PI) controller, while the reference value for the rotor flux magnitude is set to a constant value which can be limited if field-weakening operation is desired. Reference values are denoted with a star superscript: $(*)^*$.

In FOC the PI controllers for both the field- (d) and torque-producing (q) currents are operating in the dq coordinate system which is aligned with the rotor flux. However, for the enumeration-based predictive current control (PCC) algorithm the control task is executed in the stationary $\alpha\beta$ system; in order to do the enumeration in dq coordinates, it would be necessary to transform all possible voltage vectors to this system, too. Thus, it is computationally cheaper to transform the current references i_{sd}^* and i_{sq}^* to the $\alpha\beta$ coordinate system. For this operation the rotor flux angle φ has to be calculated. Besides, the rotor flux $\boldsymbol{\psi}_\mathrm{r}$ is also necessary to estimate the back-EMF voltage $\boldsymbol{v}_\mathrm{emf}$. Furthermore, the dc-link capacitor voltages v_c1 and v_c2 have to be measured in order to perform the voltage balancing.

C. Heuristic Voltage Vector Preselection

In order to obtain the continuous-valued solution for the optimization problem, the voltage balancing is not considered. Thus, a linear or ℓ_1-norm cost function can be set up:

$$J_1 = |i_{\mathrm{s}\alpha}^* - i_{\mathrm{s}\alpha}(k+1)| + \left|i_{\mathrm{s}\beta}^* - i_{\mathrm{s}\beta}(k+1)\right|\,, \tag{12}$$

where k is the current sample. Since the current control loop of an IM is a two-dimensional linear first order system with the back-EMF voltages $\boldsymbol{v}_\mathrm{emf}$ which are considered as "external" disturbances, the optimization task can be solved via linear programming. However, linear programs (LPs) are also time-consuming. For this reason the calculations are done offline utilizing multiparametric programming [25], [26] with the

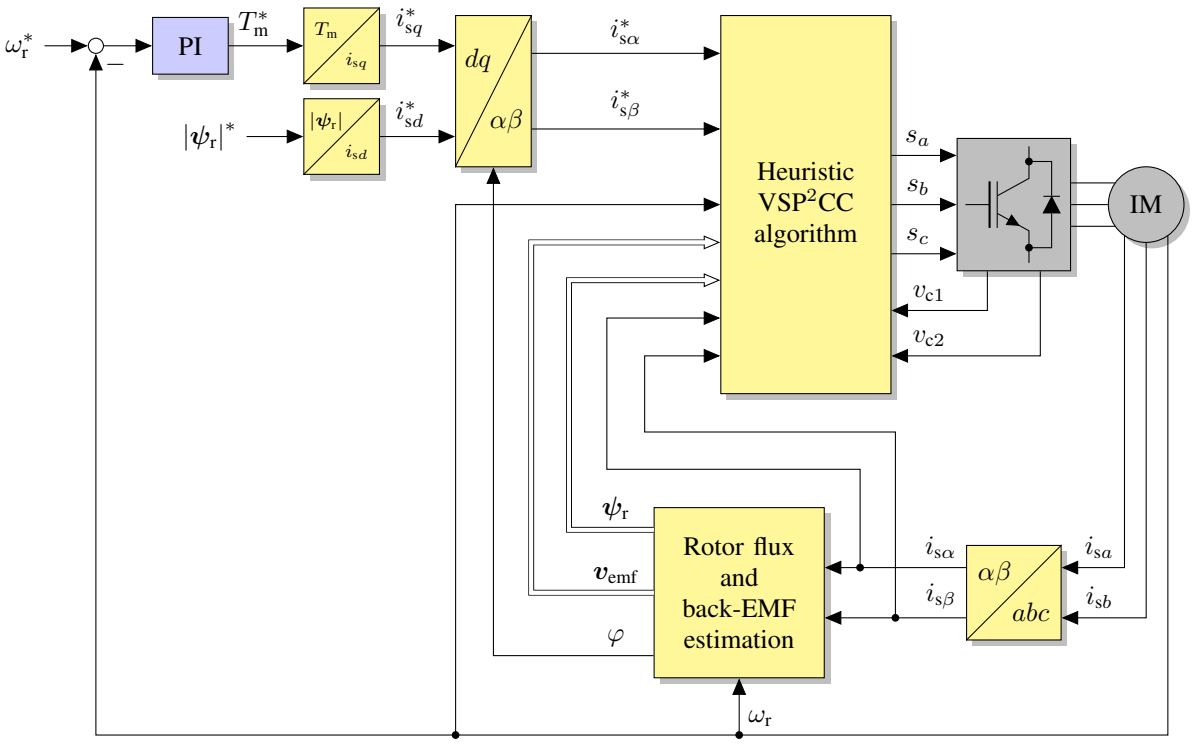

Fig. 3. Block diagram of the heuristic variable switching point predictive current controller (VSP^{2}CC).

Multiparametric Toolbox (MPT) [27] for Matlab. The system states (the $\alpha\beta$ currents $\boldsymbol{i}_\mathrm{s}(k)$, their references $\boldsymbol{i}_\mathrm{s}^*$ and the back-EMF voltages $\boldsymbol{v}_\mathrm{emf}(k)$) are used as parameters. After the offline solution is calculated, a six-dimensional polytope structure can be obtained. In every polytope a certain piecewise affine control law is valid. Finding the optimal solution for the LP then reduces to a simple search for the correct region in state space. However, as the obtained number of polytopes is usually quite high, an exhaustive search over all regions would not be feasible in real-time. For this reason a binary search tree according to [28] is created. This binary search tree makes an efficient region search possible, even in real-time.

The heuristic preselection strategy is based on the assumption that the discrete-valued optimum is normally close to the continuous-valued optimum. Because of this, for every predicted time step only the three closest voltage vectors with respect to the continuous optimum are used for the optimization. The $\alpha\beta$ plane with the 19 voltage vectors in Fig. 2 can be divided into 24 regions. After the determination of the correct region only the three voltage vectors at its corners are taken into account for the following discrete-valued optimization (instead of all 19 ones).

Basically, the region can be determined in the same way as for space vector modulation (SVM). However, for multilevel inverters it can become a quite complex issue to find the correct sector in which the optimal continuous voltage vector lies. Basically, the same strategies to detect the sector which are used for SVM can be applied as well. By taking a closer look at the voltage vectors in Fig. 2, it can be seen that all regions are triangles which also holds true for multilevel inverters. Triangles are nothing else than convex polytopes. Because of this the region can also be found using a binary search tree.

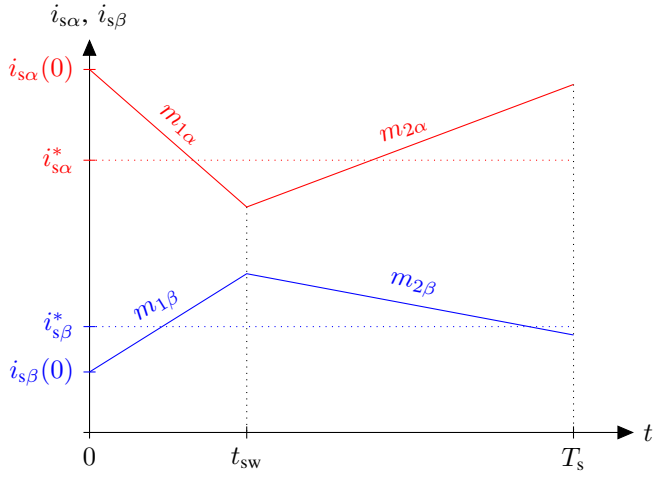

Fig. 4. Principle of the VSP calculation.

D. Calculation of the Variable Switching Point

Fig. 4 illustrates the basic principle of the VSP calculation. The squared rms current error is given by

$$e_{\mathrm{rms}^2} = \frac{1}{T_\mathrm{s}} \left(\int_0^{t_\mathrm{sw}} (\boldsymbol{i}_\mathrm{s}^* - \boldsymbol{i}_\mathrm{s}(t))^2 \mathrm{d}t + \int_{t_\mathrm{sw}}^{T_\mathrm{s}} (\boldsymbol{i}_\mathrm{s}^* - \boldsymbol{i}_\mathrm{s}(t))^2 \mathrm{d}t \right) , \quad (13)$$

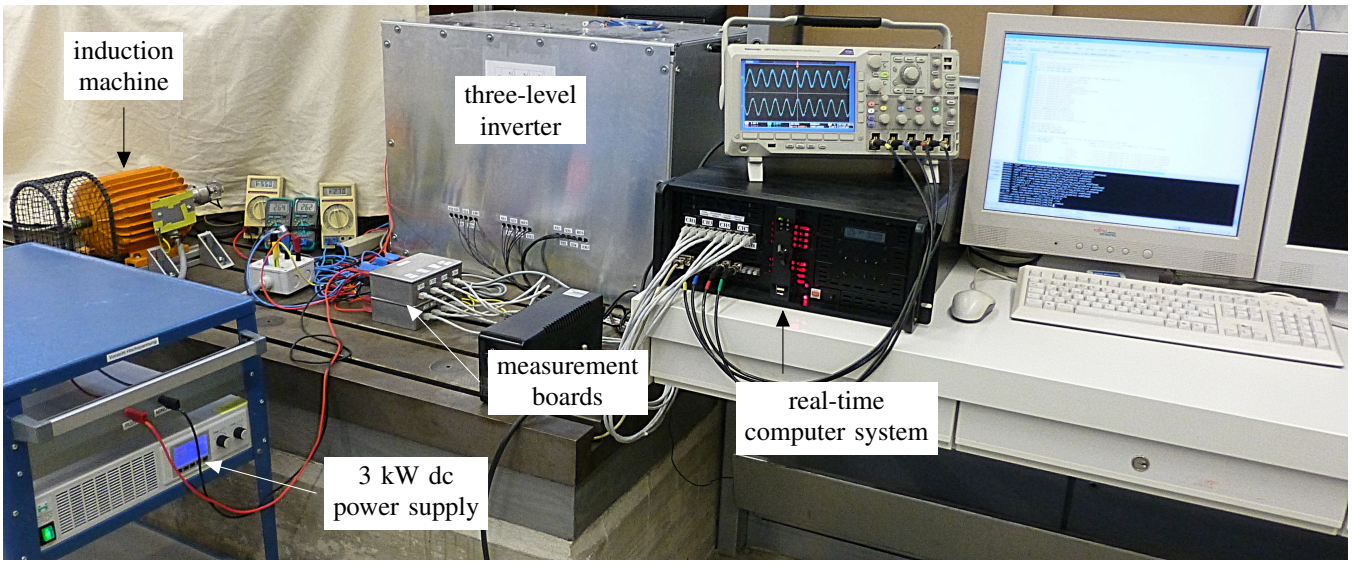

Fig. 5. Complete test bench with the dc power supply, three-level NPC inverter, real-time computer system and IM.

where $\boldsymbol{i}_\mathrm{s}^*$ is the current reference and t_sw is the variable switching point. Note that $\boldsymbol{i}_\mathrm{s}$ at time instant $t = 0$ is the measured stator current. In order to simplify the calculations, it is assumed that the current slopes are constant over the whole sample. The current slopes can easily be calculated by doing another set of predictions; one for the currently applied voltage vector (which will be kept until t_sw is reached) and the one which has to be tested.

After some calculations, the VSP can be calculated such that the squared rms current error is minimized; the final equation for t_sw results to

$$t_\mathrm{sw} = \frac{A + B}{C + D}\,, \tag{14}$$

with

$$\begin{aligned} A &= (m_{2\alpha} - m_{1\alpha})(2i_{\mathrm{s}\alpha}(0) - 2i_{\mathrm{s}\alpha}^* + T_\mathrm{s} m_{2\alpha})\,, \\ B &= (m_{2\beta} - m_{1\beta})(2i_{\mathrm{s}\beta}(0) - 2i_{\mathrm{s}\beta}^* + T_\mathrm{s} m_{2\beta})\,, \\ C &= (m_{1\alpha} - m_{2\alpha})(2m_{1\alpha} - m_{2\alpha})\,, \text{ and} \\ D &= (m_{1\beta} - m_{2\beta})(2m_{1\beta} - m_{2\beta})\,, \end{aligned}$$

where m_1 are the current slopes of the currently applied voltage vector and m_2 those of the new voltage vector which is tested.

E. Final Optimization and Voltage Balancing

When the VSP for a tested voltage vector/switching state (from the heuristically reduced set of voltage vectors) has been calculated, an ℓ_2-norm (quadratic) cost function is used for the final optimization:

$$\begin{aligned} J_2 = (\boldsymbol{i}_\mathrm{s}^* - \boldsymbol{i}_\mathrm{s}(k + n_\mathrm{int}))^2 + \lambda \Delta v_\mathrm{c}(k + n_\mathrm{int})^2 + \\ + (\boldsymbol{i}_\mathrm{s}^* - \boldsymbol{i}_\mathrm{s}(k+1))^2 + \lambda \Delta v_\mathrm{c}(k+1)^2\,, \end{aligned} \tag{16}$$

where $n_\mathrm{int} = t_\mathrm{sw}/T_\mathrm{s} \in [0, 1]$, and λ is the weighting factor for the voltage balancing.

Because of the reduced set of voltage vectors it has to be checked if the dc-link capacitor voltages can still be balanced. The sum of all three phase currents is zero (balanced circuit) and positive and negative switching states do not affect the voltage balancing. Thus, no matter which zero switching state (ppp, 000 or nnn) is chosen, the voltage balance will not be affected. By taking a closer look at the voltage vectors on the inner hexagon in Fig. 2, one of the two possible switching states produces one zero switching state in one phase, the other possible switching state applies two zero switching states but in the *other* two phases. Because of this the voltage balancing for these voltage vectors can be done by choosing the appropriate switching state. Considering the outer hexagon, the switching states at the corners (pnn, ppn, npn etc.) do not affect the capacitor voltage. Thus, the only remaining switching states which can lead to voltage unbalances are p0n, 0pn, np0, n0p, 0np and pn0. However, it can also be seen that all these voltage vectors belong to regions which also contain voltage vectors of the inner hexagon—because of this the voltage balance can be ensured despite the heuristically reduced set of voltage vectors.

IV. Experimental Results

Several experiments have been performed in order to verify the proposed control algorithm and to demonstrate its potentials. The experimental setup shown in Fig. 5 consists of a three-level NPC inverter driving a 2.2 kW squirrel-cage IM whose parameters are shown in Table I. The real-time computer system is an improved version of the one described in [29] with a 3.4 GHz Pentium 4 CPU [30].

Fig. 6 shows the transient response of the proposed control algorithm. For this reason the speed reference was stepped down from 2000 rpm to 1000 rpm at time $t \approx 40$ ms. As it can be seen in Fig. 6, the speed reference change results in a step change of both stator currents. It is clearly visible that the controller has no problems to track its references. After the normal delay of two samples (one due to the calculations and one resulting from the fact that the optimization has to

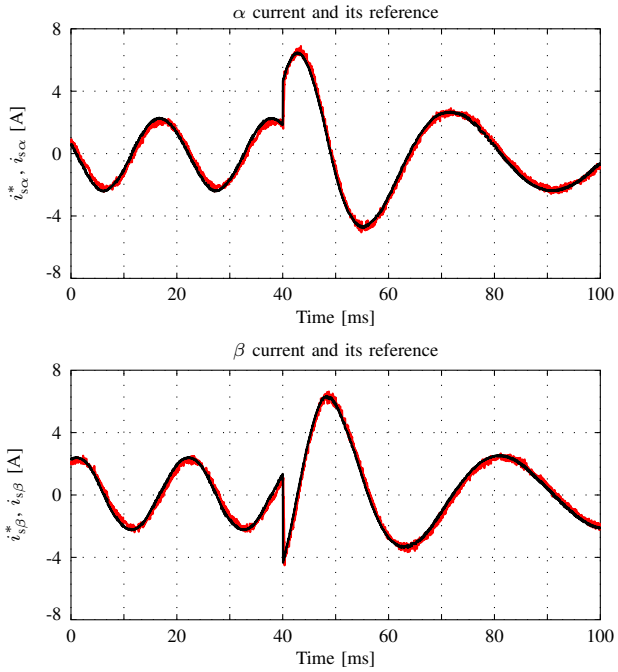

(a) (Larger time scale) Top: α component of current (red line) and its reference (black line). Bottom: β component of current (red line) and its reference (black line).

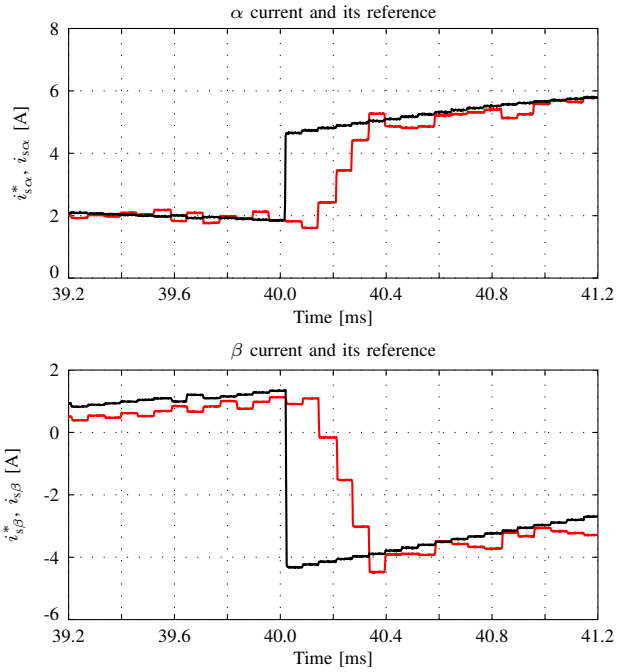

(b) (Detail during reference step) Top: α component of current (red line) and its reference (black line). Bottom: β component of current (red line) and its reference (black line).

Fig. 6. Experimental results of a three-level NPC inverter driving an IM for a step change in the speed reference at $t \approx 40\,\text{ms}$.

TABLE I
PARAMETERS OF THE INDUCTION MACHINE

Parameter	Value
Nominal power P_{nom}	2.2 kW
Synchronous frequency f_{syn}	50 Hz
Nominal current $\lvert\boldsymbol{i}_{\text{s,nom}}\rvert$	8.5 A
Power factor $\cos(\varphi)$	0.86
Nominal speed ω_{nom}	2830 rpm
Number of pole pairs p	1
Stator resistance r_{s}	2.1294 Ω
Rotor resistance r_{r}	2.2773 Ω
Stator inductance l_{s}	350.47 mH
Rotor inductance l_{r}	350.47 mH
Mutual inductance l_{m}	340.42 mH
Inertia J	0.002 $\frac{\text{kg}}{\text{m}^2}$

be performed for the next sample) the currents quickly follow their references within three samples.

The second experiment was conducted in order to compare the steady-state currents at 100 rpm for the proposed strategy to a predictive current control (PCC) strategy without a variable switching point. The experiment was conducted with a sampling interval of $T_{\text{s}} = 62.5\,\mu\text{s}$. The result can be seen in Fig. 7. It is clearly visible that the proposed control algorithm has a significant influence on the quality of the controlled currents. At this operating point the VSP^{2}CC strategy can operate with a much higher switching frequency ($f_{\text{sw}} \approx 1.9\,\text{kHz}$) than the conventional PCC algorithm ($f_{\text{sw}} \approx 850\,\text{Hz}$). This higher switching frequency results in less current ripples at this operating point. The same experiment was repeated at full nominal speed (2830 rpm). The results can be seen in Fig. 8. At this operating point the VSP^{2}CC strategy (Fig. 8(a)) leads to nearly the same switching frequency as plain PCC (Fig. 8(b)) and the current ripples are in the same range.

Finally, the results of the last experiment are shown in Fig. 9. It was conducted in order to investigate more deeply the effect of the VSP^{2}CC strategy on the switching frequency depending on the operation point of the system. Thus, the average IGBT switching frequency was measured in steps of 10 rpm from 0 rpm to full nominal speed (2830 rpm) for both control methods. It is clearly visible that VSP^{2}CC leads to much higher switching frequencies at low machine speeds and thus also to decreased current ripples. While the switching frequency for VSP^{2}CC is always higher than 900 Hz, it goes down to less than 100 Hz for the conventional PCC algorithm. As verified in the previous experiment, for higher machine speeds the switching frequencies are nearly the same for both strategies.

V. Conclusion and Further Work

In this paper a variable switching point predictive current control (VSP^{2}CC) of induction motors (IMs) with heuristic voltage vector preselection was introduced. It provides an effective solution for the two main drawbacks of enumeration-

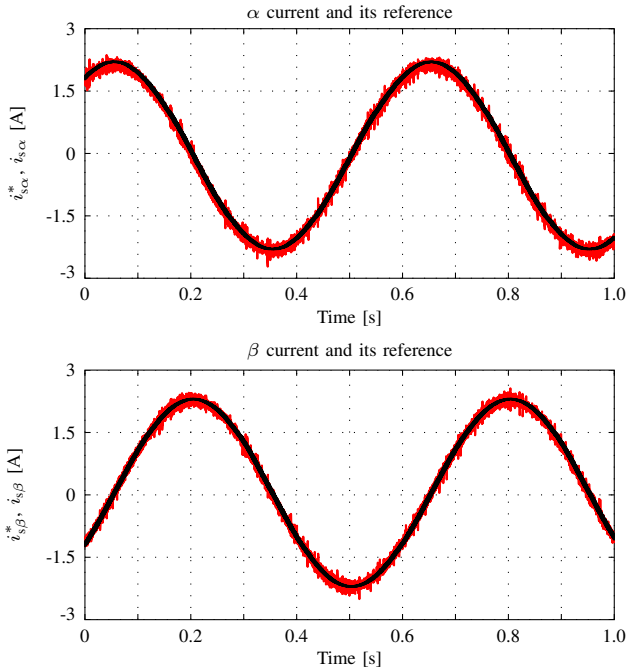

(a) Top: α component of current (red line) and its reference (black line). Bottom: β component of current (red line) and its reference (black line).

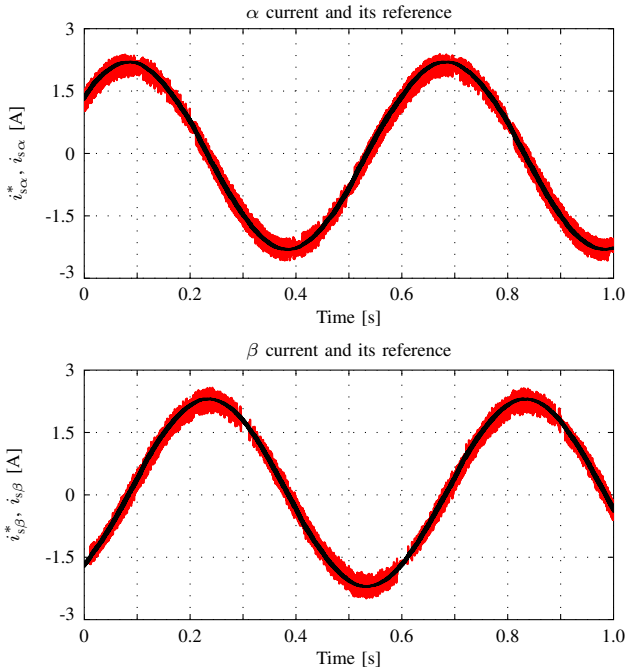

(b) Top: α component of current (red line) and its reference (black line). Bottom: β component of current (red line) and its reference (black line).

Fig. 7. Experimental results of current in the $\alpha\beta$ plane at steady-state operation at 100 rpm produced by (a) the proposed strategy (VSP^{2}CC—$f_{sw} \approx 1.9$ kHz), and by (b) an MPC strategy where a VSP is not calculated (PCC—$f_{sw} \approx 0.85$ kHz).

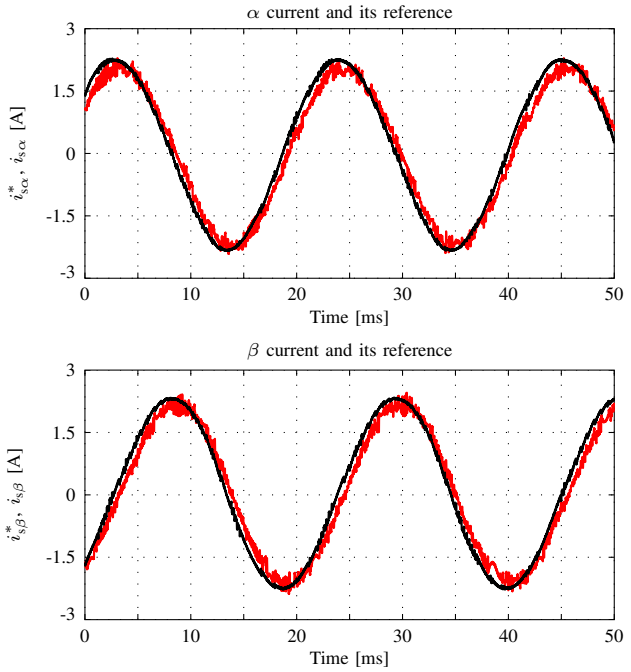

(a) Top: α component of current (red line) and its reference (black line). Bottom: β component of current (red line) and its reference (black line).

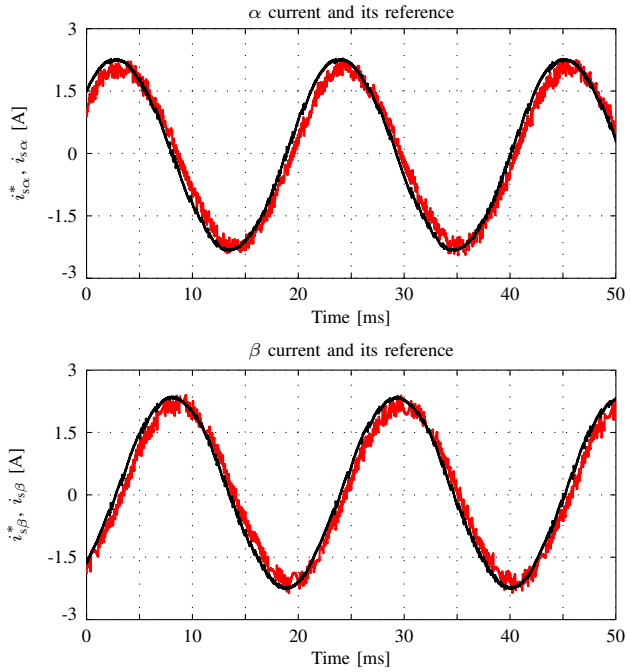

(b) Top: α component of current (red line) and its reference (black line). Bottom: β component of current (red line) and its reference (black line).

Fig. 8. Experimental results of current in the $\alpha\beta$ plane at steady-state operation at 2830 rpm produced by (a) the proposed strategy (VSP^{2}CC—$f_{sw} \approx 2.1$ kHz), and by (b) an MPC strategy where a VSP is not calculated (PCC—$f_{sw} \approx 1.65$ kHz).

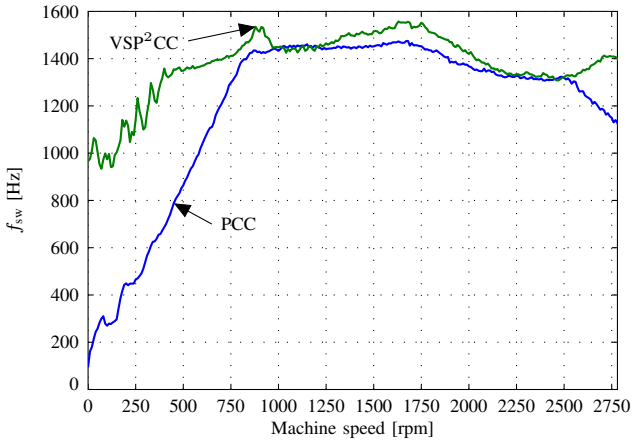

Fig. 9. Average switching frequency of VSP^{2}CC (green line) and PCC (blue line) ($T_s = 100\,\mu$s).

based model predictive control (MPC) methods, i.e. the high calculation effort and large ripples on the controlled variables. The experimental results clearly verify that the controller shows excellent behavior during transients and in steady-state. Further developments of the proposed method are the extension to five-level inverters.

REFERENCES

[1] M. P. Kazmierkowski, R. Krishnan, and F. Blaabjerg, *Control in Power Electronics*. New York: Academic Press, 2002.

[2] I. Takahashi and T. Noguchi, "A new quick-response and high-efficiency control strategy of an induction motor," *IEEE Trans. Ind. Appl.*, vol. IA-22, no. 5, pp. 820–827, Sep. 1986.

[3] M. Depenbrock, "Direct self-control (DSC) of inverter-fed induction machines," *IEEE Trans. Power Electron.*, vol. 3, no. 4, pp. 420–429, Oct. 1988.

[4] J. M. Maciejowski, *Predictive Control with Constraints*. Englewood Cliffs, NJ: Prentice-Hall, 2002.

[5] J. B. Rawlings and D. Q. Mayne, *Model Predictive Control: Theory and Design*. Madison, WI: Nob Hill, 2009.

[6] P. Correa, M. Pacas, and J. Rodríguez, "Predictive torque control for inverter-fed induction machines," *IEEE Trans. Ind. Electron.*, vol. 54, no. 2, pp. 1073–1079, Apr. 2007.

[7] H. Miranda, P. Cortés, J. I. Yuz, and J. Rodríguez, "Predictive torque control of induction machines based on state-space models," *IEEE Trans. Ind. Electron.*, vol. 56, no. 6, pp. 1916–1924, Jun. 2009.

[8] T. Geyer, G. Papafotiou, and M. Morari, "Model predictive direct torque control—Part I: Concept, algorithm and analysis," *IEEE Trans. Ind. Electron.*, vol. 56, no. 6, pp. 1894–1905, Jun. 2009.

[9] G. Papafotiou, J. Kley, K. G. Papadopoulos, P. Bohren, and M. Morari, "Model predictive direct torque control—Part II: Implementation and experimental evaluation," *IEEE Trans. Ind. Electron.*, vol. 56, no. 6, pp. 1906–1915, Jun. 2009.

[10] T. Geyer, N. Oikonomou, G. Papafotiou, and F. D. Kieferndorf, "Model predictive pulse pattern control," *IEEE Trans. Ind. Appl.*, vol. 48, no. 2, pp. 663–676, Mar./Apr. 2012.

[11] N. Oikonomou, C. Gutscher, P. Karamanakos, F. Kieferndorf, and T. Geyer, "Model predictive pulse pattern control for the five-level active neutral point clamped inverter," in *Proc. IEEE Energy Convers. Congr. Expo.*, Raleigh, NC, Sep. 2012, pp. 129–136.

[12] T. Geyer, "Model predictive direct current control: Formulation of the stator current bounds and the concept of the switching horizon," *IEEE Ind. Appl. Mag.*, vol. 18, no. 2, pp. 47–59, Mar./Apr. 2012.

[13] T. Geyer and S. Mastellone, "Model predictive direct torque control of a five-level ANPC converter drive system," *IEEE Trans. Ind. Appl.*, vol. 48, no. 5, pp. 1565–1575, Sep./Oct. 2012.

[14] T. Geyer, "Low complexity model predictive control in power electronics and power systems," Ph.D. dissertation, Autom. Control Lab. ETH Zurich, Zurich, Switzerland, 2005.

[15] P. Cortés, M. P. Kazmierkowski, R. M. Kennel, D. E. Quevedo, and J. Rodríguez, "Predictive control in power electronics and drives," *IEEE Trans. Ind. Electron.*, vol. 55, no. 12, pp. 4312–4324, Dec. 2008.

[16] A. Linder, R. Kanchan, R. Kennel, and P. Stolze, *Model-based Predictive Control of Electric Drives*. Göttingen, Germany: Cuvillier Verlag, 2010.

[17] P. Karamanakos, "Model predictive control strategies for power electronics converters and ac drives," Ph.D. dissertation, Elect. Mach. and Power Electron. Lab. NTU Athens, Athens, Greece, 2013.

[18] P. Stolze, P. Landsmann, R. Kennel, and T. Mouton, "Finite-set model predictive control with heuristic voltage vector preselection for higher prediction horizons," in *Proc. Eur. Power Electron. Conf.*, Birmingham, UK, Aug./Sep. 2011, pp. 1–9.

[19] P. Stolze, M. Tomlinson, R. Kennel, and T. Mouton, "Heuristic finite-set model predictive current control for induction machines," in *Proc. IEEE Energy Convers. Congr. Expo. Asia*, Melbourne, Australia, Jun. 2013, pp. 1221–1226.

[20] P. Karamanakos, P. Stolze, R. Kennel, S. Manias, and T. Mouton, "Variable switching point predictive torque control," in *Proc. IEEE Int. Conf. Ind. Technol.*, Cape Town, South Africa, Feb. 2013, pp. 422–427.

[21] P. Stolze, P. Karamanakos, R. Kennel, S. Manias, and T. Mouton, "Variable switching point predictive torque control for the three-level neutral point clamped inverter," in *Proc. Eur. Power Electron. Conf.*, Lille, France, Sep. 2013.

[22] G. Patsakis, P. Karamanakos, P. Stolze, S. Manias, R. Kennel, and T. Mouton, "Variable switching point predictive torque control for the four-switch three-phase inverter," in *Proc. IEEE Int. Symp. on Pred. Control of Electr. Drives and Power Electron.*, Munich, Germany, Nov. 2013.

[23] P. Kovács, *Transient Phenomena in Electrical Machines*. Amsterdam, Netherlands: Elsevier Sci., 1984.

[24] J. Holtz, "The representation of ac machine dynamics by complex signal flow graphs," *IEEE Trans. Ind. Electron.*, vol. 42, no. 3, pp. 263–271, Jun. 1995.

[25] E. Pistikopoulos, M. C. Georgiadis, and D. Vivek, *Multi-Parametric Programming*, ser. Process Syst. Eng. Weinheim, Germany: Wiley, 2007, vol. 1.

[26] ——, *Multi-Parametric Model-Based Control*, ser. Process Syst. Eng. Weinheim, Germany: Wiley, 2007, vol. 2.

[27] M. Kvasnica, P. Grieder, M. Baotić, and M. Morari, "Multi parametric toolbox (MPT)," in *Hybrid Syst.: Comput. and Control*, ser. LNCS, R. Alur and G. Pappas, Eds. Springer-Verlag, 2004, vol. 2993, pp. 448–462, http://control.ee.ethz.ch/~mpt.

[28] P. Tøndel, T. A. Johansen, and A. Bemporad, "Evaluation of piecewise affine control via binary search tree," *Automatica*, vol. 39, no. 5, pp. 945–950, May 2003.

[29] N. Al-Sheakh Ameen, A. A. Naassani, and R. M. Kennel, "Design of a digital system dedicated for electrical drive applications," *EPE J.*, vol. 20, no. 4, pp. 37–44, Dec. 2010.

[30] P. Stolze, J. Jung, W. Ebert, and R. Kennel, "FPGA-basiertes Echtzeitrechner-System mit RTAI-Linux für Antriebssysteme," in *Proc. SPS Drives Kongr.*, Nuremberg, Germany, Nov. 2013.